Int. J. Heat Mass Transfer. Vol. 34, No. 7, pp. 1593–1603, 1991
Printed in Great Britain

0017-9310/91 $3.00+0.00

Unsteady heat and mass transfer with phase changes in an insulation slab: frosting effects

Y.-X. TAO, R. W. BESANT and K. S. REZKALLAH
Department of Mechanical Engineering, University of Saskatchewan, Saskatoon, Sask., Canada S7N 0W0

(*Received* 24 *April* 1990 *and in final form* 6 *August* 1990)

Abstract—Moisture and frost accumulation in a glass-fiber slab are analyzed, using a one-dimensional, transient, vapor diffusion model with phase changes and variable properties. The cold sink boundary is impermeable and subject to a temperature below the triple point of water while the opposing warm boundary is open to a convective moist air. The numerical results are presented for moisture/frost accumulation under various conditions. It is shown that the motion of the frozen boundary is primarily governed by thermal diffusion. The effects of moisture/frost accumulation on thermal performance are also discussed.

1. INTRODUCTION

HEAT AND moisture transport through insulation materials has drawn substantial attention among researchers because of the many practical applications for energy management for building and refrigerated envelopes. Extensive studies [1–3] have been conducted to analyze simultaneous heat and mass transfer for various systems, along with a few experimental efforts [4, 5]. In recent years, condensation effects in insulation have been investigated rigorously [6, 7] for applied temperature ranges above the freezing point. However, there are many applications in which the cold side temperature of an insulation layer can be below the triple point of water. In these applications, condensed water inside the insulation (if any) may exist as frost in places where the temperature is below the freezing temperature. Therefore, it is possible that the dry, wet, and frozen regions coexist in the slab. Little effort has been made so far to analyze the heat and moisture transfer processes with both condensation and frosting effects in insulation materials, although some studies on frosting and freezing processes in porous media may be related [8–10].

It is understood that the main mechanisms involved in heat and moisture transfer in fibrous insulation with no air infiltration due to air pressure difference (e.g. a vapor retarder is used), are:

- vapor diffusion and natural convection in the gas phase due to density variation induced by temperature and vapor concentration gradients;
- phase changes such as condensation (or evaporation), freezing (or thawing), and ablimation (or sublimation).

Moisture and frost accumulation leads to an alteration of the temperature field due to physical effects predicted by thermodynamic phase-equilibrium relations and also results in an increase in the effective thermal conductivity of an insulation material. These effects augment heat loss through insulation materials.

In this study, the focus is on the analysis of transient and spatial variations of moisture/frost content as a result of temperature and vapor concentration gradients across a typical fibrous slab and the augmented heat transfer due to phase change. The approach is similar to the study of Vafai and Sarker [6], who used the local volume average technique, which is modified in this study and applied to the case with temperature below the triple point of water. The wet–frozen boundary is found directly from the solution of the governing equations by the numerical method. It is this boundary that changes the distribution of moisture as compared to the case without frosting. For processes with only condensation effects, it has been reported [3] that when the time scale for the motion of the dry–wet boundary in porous media is much larger than the thermal diffusion time scale (which is only true for fairly wet media), the position of the moving boundary can be found from a quasi-steady-state solution. This may not be applicable to the cases with frosting and small moisture accumulation. We expect that for initially dry insulation and small Lewis numbers (defined by the ratio of the effective thermal and mass diffusivities), the position of the moving frozen boundary is primarily governed by thermal diffusion. This would lead to the exclusion of moving boundary conditions in our finite difference formulation. In order to justify this, a time scale for the motion of the boundary between the wet and frozen regions will be developed.

2. ANALYSIS

The problem is formulated using the local averaging technique. At any location in space z, a quantity y is said to be 'spatially averaged' when it is defined as

NOMENCLATURE

Bi	Biot number, $h_a L/k^*_{\text{eff}}$
Bi_m	mass transfer Biot number, $h_m L/D^*_{\text{v,eff}}$
c_p	heat capacity at constant pressure
D	mass diffusivity, dimensional
$D^*_{\text{v,eff}}$	effective vapor diffusivity, $\varepsilon_\gamma D/\tau$
Fo	Fourier number, $\alpha^*_{0,\text{eff}} t^*/L^2$
h_{fg}	enthalpy of vaporization
h_{sf}	enthalpy of fusion
h_{sg}	enthalpy of sublimation
k	thermal conductivity
L	characteristic length of the slab, dimensional
$\dot{m}$	rate of phase change
p	pressure
Q'	heat flux ratio defined in equation (21)
R_v	vapor gas constant
t	time
T	temperature
ΔT	reference temperature difference, $T^*_a - T^*_c$
z	coordinate axis.

Greek symbols

$\alpha^*_{0,\text{eff}}$	effective thermal diffusivity, $k_{0,\text{eff}}/\rho^*_0 c^*_0$
ε	volume fraction
ρ	density
τ	tortuosity
ϕ	relative humidity.

Subscripts

a	air
c	cold
D	diffusion
f	frozen region
ref	reference
s	saturated
t	total
v	vapor phase
w	wet region
β	liquid phase in wet region or ice phase in frozen region
γ	gas phase which consists of air and water vapor
σ	solid phase
0	initial; reference for non-dimensional scales (Tables 1 and 2).

Superscripts

~	time average
*	dimensional.

$$\langle y\rangle(z) = \frac{1}{V(z)}\int_{V(z)} y\,\mathrm{d}V \tag{1}$$

where V is the total volume of a small elementary control volume. A quantity in phase α is said to be 'intrinsic phase averaged' when it is defined as

$$\langle y\rangle^\alpha = \frac{1}{V_\alpha(t)}\int_{V_\alpha(t)} y_\alpha\,\mathrm{d}V. \tag{2}$$

One is referred to Whitaker's work [11] for the detailed derivation of the governing equations for general heat and mass transfer in porous media. In this study, the averaging symbols are omitted in order to simplify the notation. The equations for condensation and frosting in fibrous insulation are essentially the same as those in ref. [6] for the condensation problem with Peclet number equal to zero, except here the β phase is defined as the liquid phase in the wet region of the slab and as the second solid phase (ice) in the frozen region.

The following assumptions are made to arrive at the governing equations: (a) the total gas phase (water vapor plus air) pressure in the insulation matrix is constant; (b) the insulation material is homogeneous and isotropic; (c) the insulation matrix solid–liquid–gas region and the solid–frost–gas region are close to local thermal equilibrium and as a consequence, only sublimation or ablimation is considered in the frozen region; (d) the liquid is in the pendular state; (e) no convective gas phase flow occurs in the insulation matrix; i.e. any moisture accumulation is caused by vapor diffusion only; and (f) in the frozen region, frost does not exist as a self-porous medium. Assumptions (a)–(c) have been used previously in the analysis of insulation materials [6, 7] and assumptions (d) and (e) are based on the boundary and initial conditions considered in this study. Assumption (f) is justified for small amounts of frost accumulation which is true for diffusion controlled processes.

2.1. *Governing equations*

The following coupled, non-linear partial differential equations (non-dimensionalized according to the definitions listed in Tables 1 and 2) are used to describe the transport phenomena:

β phase continuity equation

$$\frac{\partial \varepsilon_\beta}{\partial t} + \frac{\dot{m}}{P_1} = 0 \tag{3}$$

gas diffusion equation

$$\frac{\partial(\varepsilon_\gamma \rho_v)}{\partial t} - \dot{m} = \frac{\partial}{\partial z}\left(\Psi_D \frac{\partial \rho_v}{\partial z}\right) \tag{4}$$

energy equation

$$\rho c_p \frac{\partial T}{\partial t} + \dot{m} P_4 = \frac{\partial}{\partial z}\left(k_{\text{eff}} \frac{\partial T}{\partial z}\right) \tag{5}$$

where P_1 in equation (3) and P_4 in equation (5) may

Table 1. Dimensionless variables

ρ	c_p	T	ρ_i	k_i	p_i	z	c_i	k_{eff}	t	$\dot{m}$
ρ^*/ρ_0^*	c_p^*/c_0^*	$T^*/\Delta T^*$	ρ_i^*/ρ_0^*	$k_i^*/k_{0,\text{eff}}^*$	$p_i^*/p_{v,0}^*$	z^*/L	c_i^*/c_0^*	$k_{\text{eff}}^*/k_{0,\text{eff}}^*$	$t^*/(L^2/\alpha_{0,\text{eff}}^*)$	$\dot{m}^*/(\rho_0^*\alpha_{0,\text{eff}}^*/L^2)$

Table 2. Dimensionless parameters

Ψ_D	P_1	P_4	P_8	P_{10}	P'_1	P'_4	P'_{10}	P'_{11}
$D_{v,\text{eff}}^*/\alpha_{0,\text{eff}}^*$	ρ_β^*/ρ_0^*	$h_{fg}^*/c_0^*\Delta T^*$	$\Delta T^* R_v^* \rho_0^*/p_{v,0}^*$	$h_{fg}^*/R_v^*\Delta T^*$	$\rho_\beta^*(\text{ice})/\rho_0^*$	$h_{sg}^*/c_0^*\Delta T$	$h_{sg}^*/R_v^*\Delta T^*$	$\Delta T^* R_a^* \rho_0^*/p_{v,0}^*$

be replaced by P'_1 and P'_4, respectively, for the frozen region (see Table 2), and $\dot{m}$ is the dimensionless mass rate of phase change per unit volume. The constitutive equations are:

volumetric constraint

$$\varepsilon_\sigma + \varepsilon_\beta + \varepsilon_\gamma = 1 \tag{6}$$

thermodynamic relations

$$p_a = p_t - p_v \tag{7}$$

$$p_a = P_{11}\rho_a T \tag{8}$$

$$p_v = P_8 \rho_v T \tag{9}$$

and for saturation conditions

$$p_v = \exp\left[-P_{10}\left(\frac{1}{T} - \frac{1}{T_{\text{ref}}}\right)\right] \tag{10}$$

where

$$\rho = \varepsilon_\sigma \rho_\sigma + \varepsilon_\beta \rho_\beta + \varepsilon_\gamma(\rho_v + \rho_a) \tag{11}$$

$$c_p = \frac{\varepsilon_\sigma \rho_\sigma c_\sigma + \varepsilon_\beta \rho_\beta c_\beta + \varepsilon_\gamma(c_v \rho_v + c_a \rho_a)}{\rho} \tag{12}$$

$$k_{\text{eff}} = \varepsilon_\sigma k_\sigma + \varepsilon_\beta k_\beta + \varepsilon_\gamma \frac{k_v \rho_v + k_a \rho_a}{\rho_v + \rho_a}. \tag{13}$$

Also, in equation (10), P_{10} may be replaced by P'_{10} for the frozen region.

2.2. *Computational procedure*

The problem is modeled as a porous insulation slab with impermeable and adiabatic vertical boundaries, as shown in Fig. 1(a). The lower horizontal boundary is impermeable and subject to a cold temperature that may be below the triple point temperature of water, and the upper one is open to a convective moist air at a specified room temperature and humidity level. The boundary and initial conditions to complete the formulation are

$$\frac{\partial T(z=0,t)}{\partial z} = -Bi[T_\infty - T(z=0,t)] \tag{14}$$

$$\frac{\partial \rho_v(z=0,t)}{\partial z} = -Bi_m[\rho_\infty - \rho_v(z=0,t)] \tag{15}$$

$$T(z=1,t) = T_c \tag{16}$$

$$\rho_v(z=1,t) = \exp\left[-P'_{10}\left(\frac{1}{T_c} - \frac{1}{T_{\text{ref}}}\right)\right] \Big/ (P_8 T_c), \quad \text{if} \quad \varepsilon_\beta(z=1) \geqslant 10^{-6}$$

$$\frac{\partial \rho_v(z=1,t)}{\partial z} = 0, \quad \text{if} \quad \varepsilon_\beta(z=1) < 10^{-6} \tag{17}$$

$$T(z, t=0) = T_0 \tag{18}$$

$$\rho_v(z, t=0) = \rho_{v0} \tag{19}$$

$$\varepsilon_\beta(z, t=0) = \varepsilon_{\beta 0}. \tag{20}$$

In equation (17), P_{10} may be used instead of P'_{10} if $T_c > 273.16$ K. At the boundary of $z = 0$, the following relation between the heat and mass transfer coefficients is used [5]:

$$h_m = \left(\frac{h_a}{1.047}\right)\left(\frac{\rho_a D_a}{k_a}\right).$$

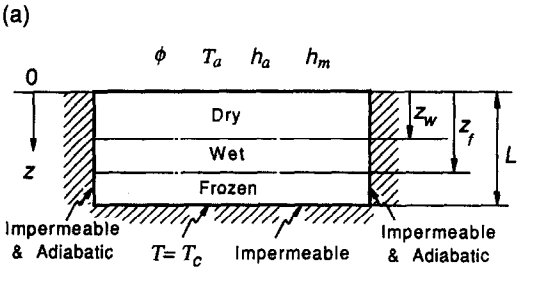

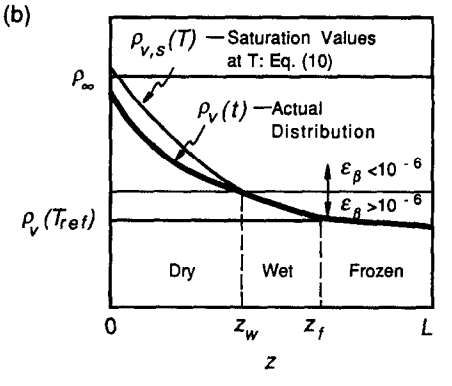

FIG. 1. (a) Transient condensation and frosting in an insulation slab with prescribed boundary conditions. (b) The definition of three possible regions in the slab: governed by water vapor density.

In order to examine the thermal performance of the insulation slab, the following heat flux ratio is defined:

$$Q' = \frac{Q_c}{Q_{c0}} = \frac{\left(-k_{eff}\frac{\partial T}{\partial z}\right)_c}{\left(-k_{eff}\frac{\partial T}{\partial z}\right)_{c0}} \quad (21)$$

where Q_c is the heat flux leaving the cold boundary and Q_{c0} the heat flux leaving the cold boundary of the same insulation slab subject to the same boundary conditions except $\varepsilon_\beta = 0$ at any time and location.

It has been reported that if $\varepsilon_\beta < 10^{-6}$, water is in the adsorbed state, therefore vapor can no longer be considered in the saturation state [4, 6, 7]. Based on this, the following three different regions are defined:

Dry region: where $\varepsilon_\beta < 10^{-6}$, and only vapor and air exist in the pores of the slab.

Wet region: where $\varepsilon_\beta > 10^{-6}$ and $T^* > 273.16$ K, and vapor, air, and liquid coexist.

Frozen region: where $\varepsilon_\beta > 10^{-6}$ and $T^* < 273.16$ K, and vapor, air, and frost coexist.

From these definitions, the boundary positions between the regions are easily found (Fig. 1(b)). Depending upon the initial $\varepsilon_{\beta 0}$ used in the calculation, it may not be necessary for the above defined three regions to exist at the same time. As will be shown later, the approximation $\varepsilon_\beta > 10^{-6}$ is accurate enough to describe the effect of moisture accumulation on the thermal performance of the insulation. It should be noted that physically, due to slight inhomogeneities in fibrous insulation, the wet–dry boundary or wet–frozen boundary cannot be a single line but has a finite volume. However, according to the local volume average technique, this fuzzy boundary 'volume' can be averaged and represented by a line (at a position z_f or z_w). The definition for the moving frozen boundary implies that it is at a place where the temperature is 273.16 K. This is true only when the motion of the boundary is dominated by thermal diffusion, which is the case in this study, as will be justified later in light of time scale discussion.

The finite difference forms of equations (3)–(5) are derived using the implicit scheme with the backward difference for the time derivative. The central difference form is used for internal nodes and the backward or forward difference used for the boundary nodes. The computational procedure is that, at each time step, the computed vapor density distribution is compared with the saturation vapor density calculated from equation (10) at the corresponding temperature. If the actual vapor density in a region is larger than, or equal to, the saturation density, the new two-phase region (wet or frozen depending on temperature) is then determined for the next time step. For the dry region, $\dot{m}$ was set to zero and equation (10) was not used. Equations (3)–(5) were solved for ε_β, T, and ρ_v, respectively. For the wet region, ρ_v was determined from equation (10). Equation (4) was used to solve for $\dot{m}$, and equations (3) and (5) were solved for ε_β and T, respectively. For the frozen region, the approach was basically the same as that for the wet region except the parameters P'_1, P'_4, and P'_{10} were used in the pertinent equations.

Table 3. Physical data

ρ_0^*	53.2 kg m^{-3}	k_σ^*	0.762 W m^{-1} K^{-1}
c_0^*	840.7 J kg^{-1} K^{-1}	ρ_β^*	999.87 kg m^{-3}
$\alpha_{0,\text{eff}}^*$	8.84×10^{-7} m^2 s^{-1}	c_β^*	4200 J kg^{-1} K^{-1}
D	2.39×10^{-5} m^2 s^{-1}	k_β^*	0.57 W m^{-1} K^{-1}
$k_{0,\text{eff}}^*$	0.037 W m^{-1} K^{-1}	ρ_β^* (ice)	917.0 kg m^{-3}
L	0.099 m	c_β^* (ice)	1924 J kg^{-1} K^{-1}
ε_σ	0.02	k_β^* (ice)	2.22 W m^{-1} K^{-1}
T_0^*	293 K	c_v^*	1882 J kg^{-1} K^{-1}
T_a^*	293 K	k_v^*	0.0247 W m^{-1} K^{-1}
T_{ref}^*	273.16 K	R_v^*	461.89 J kg^{-1} K^{-1}
h_{fg}^*	2.50×10^6 J kg^{-1}	k_a^*	0.0227 W m^{-1} K^{-1}
h_{sg}^*	1.67×10^5 J kg^{-1}	c_a^*	1005 J kg^{-1} K^{-1}
ρ_σ^*	2600 kg m^{-3}	ϕ	0.4–0.97
c_σ^*	836.8 J kg^{-1} K^{-1}	h_a	12.0 W m^{-2} K^{-1}

The accuracy of the wet–dry or wet–frozen boundary position depends on the selection of the time step and the grid size. Considering the balance between the accuracy, economy of computing time and the stability requirement, we chose $\Delta t/(\Delta z)^2 \leqslant 2.25$ with the grid size $\Delta z = 0.02$. For each time step, the difference equations were solved using the underrelaxation iteration scheme. The solution is considered to be converged when the deviation of any variable from the last iterated value is within 10^{-3}%. The physical data for fluids and the typical glass-fiber insulation slab used in modeling are summarized in Table 3.

3. THE TIME SCALE FOR THE MOTION OF THE FROZEN REGION BOUNDARY

The following approximations are used to describe the moving boundary conditions, assuming that the liquid is immobile:

$$\left.\frac{d\rho_v}{dz}\right|_f - \left.\frac{d\rho_v}{dz}\right|_w = -\rho_\beta \varepsilon_\beta Le \frac{dz_f}{dt} \quad (22)$$

$$\left.\frac{dT}{dz}\right|_f - \left.\frac{dT}{dz}\right|_w k'_{\text{eff}} = \varepsilon_\beta \Lambda \frac{dz_f}{dt} \quad (23)$$

where

$$Le = \frac{\alpha_{0,\text{eff}}^*}{D_{v,\text{eff}}}, \quad \Lambda = \frac{\rho_\beta^* h_{sf}^* \alpha_{0,\text{eff}}^*}{k_{\text{eff,f}}^* \Delta T^*}, \quad k'_{\text{eff}} = \frac{k_{\text{eff,w}}^*}{k_{\text{eff,f}}^*}.$$

By writing dT/dz terms in equation (23) as

$$\frac{dT}{dz} = \left(\frac{d\rho_v}{dz}\right)\Big/\left(\frac{d\rho_v}{dT}\right) \quad (24)$$

combining equations (22) and (23) and eliminating $(d\rho_v/dz)_w$, we have

$$\left(-\frac{dz_f}{dt}\right)=\left(-\frac{d\rho_v}{dz}\right)_f\left[\frac{\left.\frac{d\rho_v}{dT}\right|_w\Big/\left(\left.\frac{d\rho_v}{dT}\right|_f k'_{eff}\right)-1}{\rho_\beta\varepsilon_\beta\, Le+\left.\frac{d\rho_v}{dT}\right|_w \varepsilon_\beta\Lambda/k'_{eff}}\right]. \quad (25)$$

From equation (10), and also considering that at the frozen–wet interface, $T=T_{ref}$, we have

$$\left.\frac{d\rho_v}{dT}\right|_f=\frac{P'_{10}-T_{ref}}{P_8T_{ref}^3};\quad \left.\frac{d\rho_v}{dT}\right|_w=\frac{P_{10}-T_{ref}}{P_8T_{ref}^3}. \quad (26)$$

Inserting equation (26) into equation (25) yields the following expression for the moving boundary speed:

$$\left(-\frac{dz_f}{dt}\right)=\left(-\frac{d\rho_v}{dz}\right)_f\frac{1}{\rho_\beta\varepsilon_\beta\, Le}\times\left[\frac{(P_{10}-T_{ref})/(P'_{10}-T_{ref})k'_{eff}-1}{(P_{10}-T_{ref})\Lambda/(P_8T_{ref}^3k'_{eff}\rho_\beta\, Le)+1}\right]. \quad (27)$$

The quantity inside the right-hand bracket of the above equation is of the order of unity for water vapor diffusion in frost with small liquid or frost deposits and Lewis number greater than 0.01. Therefore, the dimensionless time scale for the motion of the frozen region boundary can be found from equation (27)

$$t_f=\frac{\bar{\varepsilon}_{\beta f}\rho_\beta\, Le}{\Delta\rho_v} \quad (28)$$

where $\Delta\rho_v=\rho_\infty-\rho_s(T_c)$, and $\bar{\varepsilon}_{\beta f}$ is a time averaged β phase volume fraction at the moving boundary.

The dimensionless time scale shown in equation (28) is nothing more than the ratio of the time scales for the motion of the frozen region boundary and for heat diffusion; i.e.

$$\frac{t_f^*}{L^2/\alpha^*_{eff,0}}=\frac{\bar{\varepsilon}_{\beta f}\rho_\beta^*}{\Delta\rho_v^*}Le. \quad (29)$$

Likewise, the ratio to the mass diffusive time scale is

$$\frac{t_f^*}{L^2/D^*_{v,eff}}=\frac{\bar{\varepsilon}_{\beta f}\rho_\beta^*}{\Delta\rho_v^*}. \quad (30)$$

If we follow the similar procedure in deriving equation (25) by eliminating $(d\rho_v/dz)_f$ instead of $(d\rho_v/dz)_w$, t_f may also be written as

$$t_f=\frac{z_f-z_w}{\rho_\infty-\rho_s(T_{ref})}\bar{\varepsilon}_{\beta f}\rho_\beta\, Le. \quad (31)$$

Equations (28)–(31) indicate that the time scale for the motion of the frozen region boundary is proportional to the time averaged liquid content at the boundary and inversely proportional to the vapor concentration gradient across the slab, a function of the ambient air humidity level and the cold boundary temperature. Equation (31) gives an alternative expression for t_f and shows that t_f is proportional to the length of the wet region (z_f-z_w) (see Fig. 1). The ratio of t_f to the thermal diffusive time scale is proportional to the Lewis number defined in equation (22), while the ratio of t_f to the mass diffusive time scale is independent of *Le*. As will be shown later, for many cases where vapor diffusion is the dominant mode for moisture migration, ε_β and *Le* are normally small; therefore the right-hand side of equation (29) is of the order of unity, which means the time scale for the moving boundary is essentially of the same order as that for thermal diffusion. This allows us to simply determine the moving frozen boundary position from the temperature profile and reduce the complexity of the problem. The relations between the time scales derived above will be also used to discuss the quasi-steady-state behavior of the transport processes.

4. RESULTS AND DISCUSSION

The main objective of this phase of the study is to find the distributions of moisture accumulation with the presence of a moving frozen (frost) region, and the effect of this accumulation on thermal performance of the insulation. In order to achieve this, three main parameters were varied: the ambient relative humidity, ϕ, the initial liquid volume fraction, $\varepsilon_{\beta 0}$, and the cold temperature, T_c. In all examples discussed below, the ambient temperature is kept at 293 K and the initial temperature is the same as the ambient temperature.

4.1. *Moisture and frost accumulation*

4.1.1. *Case study.* Figures 2 and 3 show the distribution of ρ_v, T, $\dot{m}$, and ε_β, with $T_c^*=253$ K and $\varepsilon_{\beta 0}=10^{-7}$ and 10^{-3}, respectively. Depending on the initial $\varepsilon_{\beta 0}$ greater or less than 10^{-6}, the vapor density distributions behave differently, which governs the different stages in the diffusion process.

(a) $\varepsilon_{\beta 0}<10^{-6}$ (Fig. 2)

Three distinguishable periods are observed:

Dry period. No frost or liquid condensation occurs in this period; i.e. $\dot{m}=0$. The vapor density at any position increases due to the inward vapor diffusion caused by the difference in vapor concentration between the ambient and inside the matrix. Heat and mass transfer are decoupled; therefore, the water vapor concentration increases due to the negative vapor concentration gradient. This period is normally very short ($Fo\leqslant 0.005$, Fig. 2(a)).

Moving freezing front period. After the vapor density is increased above the saturation density, condensation occurs, which always takes place at the cold boundary first. When the cold temperature is below 273.16 K, frost immediately starts to form and the freezing front moves towards the warm side. At the initial stage of this period, there is no wet region in the slab (see position (A) in Fig. 2(c), denoting the boundary position between the dry and frozen regions). After inward moving of the freezing front results in further decrease in the temperature in the

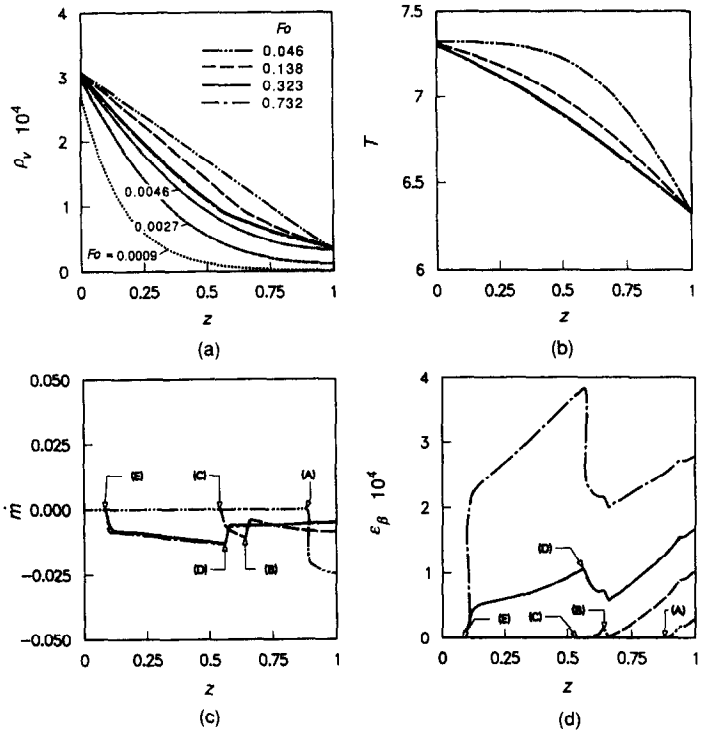

FIG. 2. The distributions of (a) ρ_v, (b) T, (c) $\dot{m}$, and (d) ε_β: $\varepsilon_{\beta 0} = 10^{-7}$, $T_c^* = 253$ K, $T_0^* = T_a^* = 293$ K, $\phi = 0.97$.

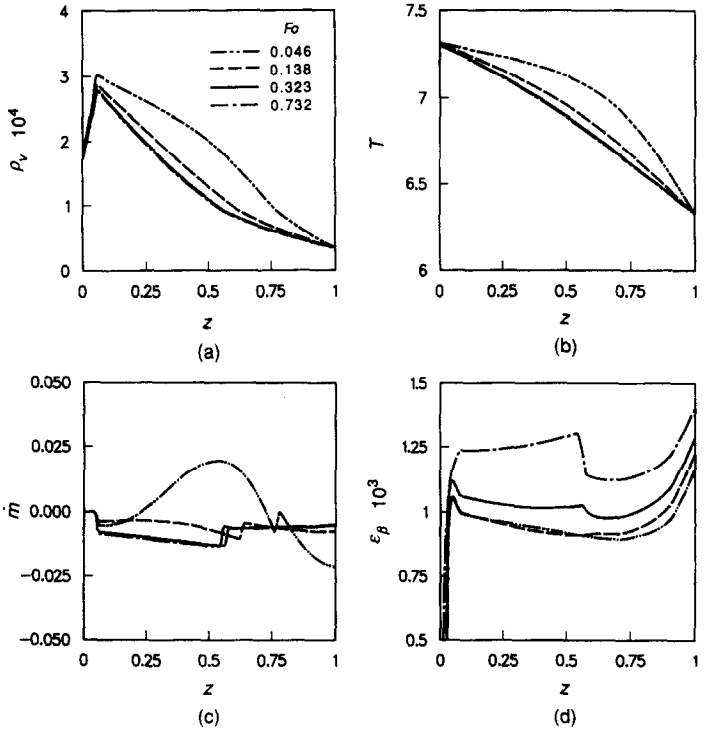

FIG. 3. The distributions of (a) ρ_v, (b) T, (c) $\dot{m}$, and (d) ε_β: $\varepsilon_{\beta 0} = 10^{-3}$, $T_c^* = 253$ K, $T_0^* = T_a^* = 293$ K, $\phi = 0.40$.

warm portion of the slab, condensation begins to take place near the freezing front. The three different phase regions can be seen in Fig. 2(c): the boundary positions were denoted by (B) (wet–frozen) and (C) (dry–wet) for $Fo = 0.1384$, and similarly by (D) and (E) for $Fo = 0.3230$. In the wet and frozen regions, mass transfer is coupled with heat transfer. The vapor density is no longer determined only by the mass diffusion process. Since the vapor density reaches its saturation value in the phase change regions, a decrease in temperature with time due to thermal diffusion results in a decrease in vapor density. In turn, the thermal energy released (or consumed) by phase changes affects the temperature distribution. As compared to the dry period, the coupling of heat and mass transfer leads to an inverse change in vapor density, i.e. the increase with time in the dry period and decrease in the moving freezing front period. This can be seen from Fig. 2(a) where $Fo \approx 0.005$ is the turning point for the change of the vapor density.

Quasi-steady-state period. The distributions in Fig. 2 show that a quasi-steady state is reached when temperature, vapor density and boundary position seem unchanged relative to the significant change in the previous periods. The asymptotic behavior in temperature and vapor density with respect to time indicates the saturation of the transient thermal, as well as mass, diffusion process. However, ε_β still increases with time, although at a very low rate, due to a non-zero distribution in $\dot{m}$ and the impermeable boundary at the cold side of the slab. The quasi-steady-state behavior allows us to estimate the moisture/frost accumulation in the quasi-steady-state period, using the following equation:

$$\varepsilon_\beta(z) = \bar{\varepsilon}_{\beta,ss}(z) + |\dot{m}|_{ss} t/P_1.$$

For the example shown in Fig. 2, $|\dot{m}|_{ss} \approx 0.012$ near the wet–frozen boundary. If we assume $\varepsilon_\beta/\varepsilon = 0.1$ is the criterion for water to be mobile, then the required time before the motion of water appears, is approximately 504 h or about 21 days. This means that moisture/frost accumulation is normally small under the diffusion-only mode.

(b) $\varepsilon_{\beta 0} > 10^{-6}$ (Fig. 3)

This condition simulates a practical insulation slab which has absorbed a certain amount of moisture due to various factors (air leakage through the wall joints, for instance), and is then subjected to a cold temperature on one side. The slab is not dry initially according to the definition. Therefore, the vapor density is assumed to obey thermodynamic relation (10) at the initial temperature. This means that there is no dry period like that in Case (a). The freezing front immediately starts to move inward. In the warm portion of the slab, evaporation takes place first due to a favorable vapor density distribution as shown in Figs. 3(a) and (c). There is only a narrow dry region confined near the surface to the moist ambient environment throughout the process (the size of the dry region depends on the ambient air humidity level; the example shown in Fig. 3 is for $\phi = 0.40$). As shown in Fig. 3(d), evaporation results in a lower ε_β in the wet region than the initial liquid volume fraction $\varepsilon_{\beta 0}$. The movement of the wet–frozen boundary, vapor diffusion and ablimation cause an increase in ε_β in the frozen region. This indicates most of the internally evaporated moisture migrates towards the cold region under a thermal gradient before the process reaches the quasi-steady state. Except for these differences, the whole process is essentially the same as the moving boundary and quasi-steady-state periods in Case (a).

4.1.2. *Comparison to the case with no frosting effects.* In Fig. 4, the result for the cold temperature above the triple point is shown. The boundary conditions used are the same as those reported in ref. [5]. Their measured quasi-steady-state temperature distribution is also plotted in Fig. 4(a), which shows a good agreement. The ε_β distribution for this case is shown in Fig. 4(b). There is a significant difference in moisture accumulation between the process with (for example, Fig. 2(d)) and without frosting. Moisture is mostly

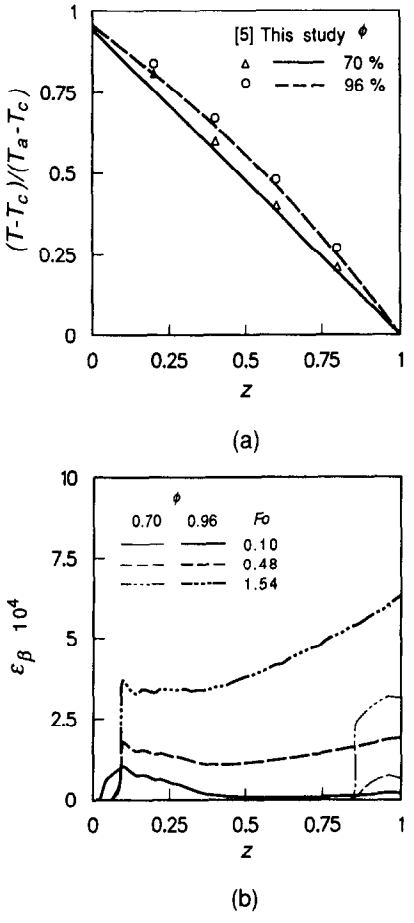

FIG. 4. (a) The quasi-steady-state temperature distribution with the same condition as ref. [5] for a condensation only process. (b) The typical ε_β distributions under the same conditions as in (a): $\varepsilon_{\beta 0} = 10^{-7}$, $T_c^* = 279.8$ K, $T_a^* = 306$ K, $\phi = 0.96$, $\rho_{slab}^* = 53$ kg m^{-3}, and $L = 66$ mm.

accumulated near the cold boundary for the process of condensation only, while in the process with a frozen cold temperature, the maximum accumulation takes place at the boundary between the frozen region and the wet region. This is because the maximum condensation rate is at the boundary when the process reaches a quasi-steady state. From equation (4), it can be seen that the discontinuity of the vapor density gradient causes a large curvature in the ρ_v curve; i.e. the spatial second derivative of ρ_v near the wet–frozen boundary causes the high rate of phase change, $\dot{m}$. Therefore, through the β phase continuity equation (3), a maximum moisture accumulation, as well as a discontinuity in ε_β, occurs at the boundary between the wet and frozen regions. Since only a small vapor diffusion flux goes in the frozen region after the quasi-steady state is reached, the wet–frozen boundary acts as a cold surface shifted into the slab by the distance $(1-z_f)$, as it can be seen that the distribution of ε_β in the wet region (Fig. 2(d)) shows a similar trend to that shown in Fig. 4(b). Generally, the wet–frozen boundary condition is controlled by the thermodynamic relation (10) which is basically the phase equilibrium behavior of water near the triple point. The discontinuity phenomenon is primarily due to the difference between heat of condensation and ablimation in equation (10) (the parameters P_{10} and P'_{10}).

4.2. *The dry, wet and frozen region boundaries*

The major difference between the transport processes with frosting effect and those without it, is the presence of a frozen region in the insulation slab, in which the thermodynamic relation between temperature and vapor concentration governs their distributions. Therefore, the size of the frozen region becomes important for determining the extent of the heat loss through the slab. Figure 5 shows the typical variations of the dry–wet boundary position, z_w, and the wet–frozen boundary position, z_f, with respect to the Fourier number. For the slab in the initially dry condition ($\varepsilon_{\beta 0} < 10^{-6}$), the wet region develops in a relatively short period (Fig. 5(a)). The position of the dry–wet boundary for the initially wet slab depends on the ambient relative humidity (0.97 in Fig. 5(b)), which imposes drying effects on the slab. The frozen boundary position is strongly dependent of the cold temperature, and is also a function of the initial liquid content. This agrees with the time scale analysis in equation (28). The time needed for moving of the frozen boundary for the slab at a lower cold temperature is shorter than that for the slab at a higher T_c. Therefore, the slab with lower T_c has a larger frozen region, as shown in Fig. 5(a). On the contrary, the influence of the initial liquid content on the frozen region length at the quasi-steady state is insignificant, although Fig. 5(b) shows that the time to reach the quasi-steady state for $\varepsilon_{\beta 0} = 10^{-2}$ is slightly longer than that for $\varepsilon_{\beta 0} = 10^{-3}$. This is because that, for the ranges of $\varepsilon_{\beta 0}$ considered in these examples, the averaged liquid contents at the wet–frozen boundary are of the same order, therefore, the time scales for the motion of the frozen boundary in these cases are also of the same order (see equation (28)). It should be noted that in this study for typical glass-fiber insulation, the Lewis number is about 0.02, and for the range studied, the diffusive time scale ratio t_f is not much larger than 1 (approximately 2–9). This means for the diffusion processes with initially dry states or small, initial liquid adsorption, and small Le, the motion of the interface cannot be decoupled from thermal diffusion. However, this decoupling might be possible for the case with a larger Le and larger moisture/frost accumulation [3].

The length of the wet region is also an important scale that affects the distributions of all parameters in the slab. From equations (28) and (31), we have

$$(z_f - z_w) \sim \frac{\rho_\infty - \rho_s(T_{ref})}{\rho_\infty - \rho_s(T_{cold})} \tag{32}$$

which indicates that, for a given cold boundary temperature, an increase in the ambient relative humidity

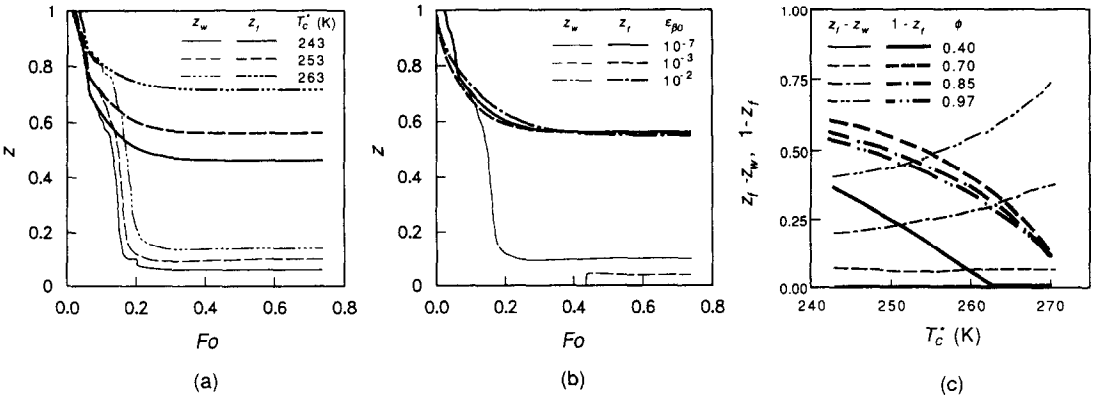

FIG. 5. The time variation of the boundary positions z_w and z_f: (a) at different T_c^* for $\varepsilon_{\beta 0} = 10^{-7}$, (b) at different $\varepsilon_{\beta 0}$ for $T_c^* = 253$ K, $\phi = 0.97$, and (c) the lengths of the wet and frozen regions under different ambient relative humidities for $\varepsilon_{\beta 0} = 10^{-7}$.

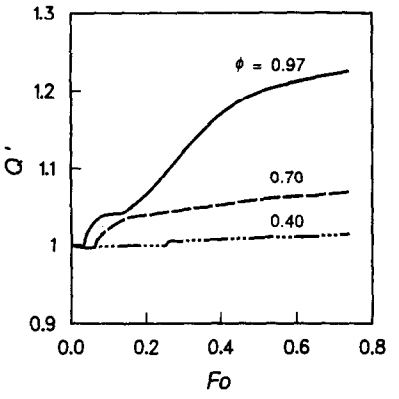

FIG. 6. The time variation of heat flux ratio at different humidity levels: $\varepsilon_{\beta 0} = 10^{-7}$, $T_c^* = 253$ K.

results in an increase in the size of the wet region. Also, under the high ambient relative humidity, the trend of the increase in the wet region size with the cold temperature becomes more pronounced, which is supported by the numerical results shown in Fig. 5(c).

4.3. *Thermal performance*

4.3.1. *Effect of relative humidity.* A calculation is carried out for the slab with an initially dry condition and otherwise the same boundary conditions, but subject to different ambient relative humidities. The obtained heat flux ratio (defined in equation (21)) is shown in Fig. 6. An increase in ambient humidity results in an increase in Q'. This is because the process is basically vapor-diffusion dominated. There is an approximately 23% increase in Q' at the quasi-steady state as relative humidity increases from 0.40 to 0.97 for the slab that is initially dry. If the slab is initially wet (i.e. $\varepsilon_{\beta 0} > 10^{-6}$), there will be more evaporation near the surface open to the ambient when the ambient humidity is at a low value. This drying effect on reducing moisture accumulation may lessen the heat loss. It should be noted that, for those examples shown in Fig. 6, the time to reach quasi-steady state is different due to the difference in the overall mass transfer potential (vapor concentration gradient across the slab).

4.3.2. *Effect of initial liquid volume fraction.* Figure 7 shows the variation of Q' with the Fourier number at different initial liquid content with otherwise the same conditions. The varying of the initial liquid volume fraction only changes the transient behavior, but does not affect the quasi-steady-state values for $\varepsilon_{\beta 0} < 10^{-3}$. In the transient period ($Fo < 0.35$), the initially wet slab has a decrease in heat loss due to internal evaporation. When the quasi-steady state is reached, those two cases shown in Fig. 7 approach one asymptote. This can be explained by means of the behavior of the moving boundaries of phase change for these processes shown in Fig. 5(b). The wet–frozen boundary positions are basically the same despite the different initial liquid contents. This implies that, as long as the initial liquid content is not large enough to cause the change of the quasi-steady-state boundary position, the temperature fields remain the same. However, for $\varepsilon_{\beta 0} = 10^{-2}$ in Fig. 7, a significant increase in Q' can be seen. This is due to an increase in effective thermal conductivity, resulting from the large liquid/frost contents in the slab (see equation (13)). The above observation leads to two important messages: (a) the approximate value 10^{-6} of ε_β for the dry–wet region criterion is a good assumption, in that a slight change of this value will not affect the results significantly, and (b) when the liquid/frost volume fractions are greater than 0.01, additional heat loss due to the increase in the effective thermal conductivity becomes significant.

4.3.3. *Effect of cold temperature.* Figure 8 shows the quasi-steady-state Q' as a function of T_c for different ϕ at given ambient temperature and heat transfer coefficient. As T_c is above the triple point temperature of water, condensation effects become important when $\phi > 0.70$, and Q' increases as T_c decreases. For the processes with both frosting and condensation effects, i.e. $T_c^* < 273$ K, Q' continues to increase as T_c^* decreases for ϕ between 0.40 and 0.90. For very high relative humidity (e.g. $\phi = 0.97$) a slight decrease in Q' is found as T_c^* decreases, which implies that there exists a transition relative humidity (say about 0.90), for which Q' might be independent of T_c^*. This may be due to the resultant effect from both the frozen region length and effective thermal conductivity. The

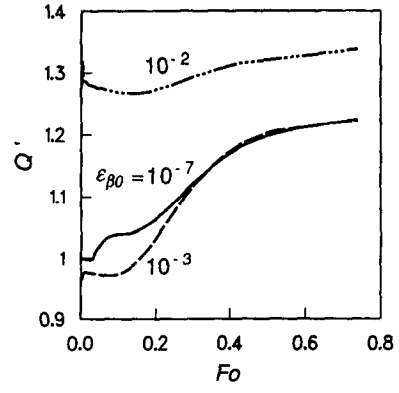

FIG. 7. The time variation of heat flux ratio at different $\varepsilon_{\beta 0}$: $T_c^* = 253$ K, $\phi = 0.97$.

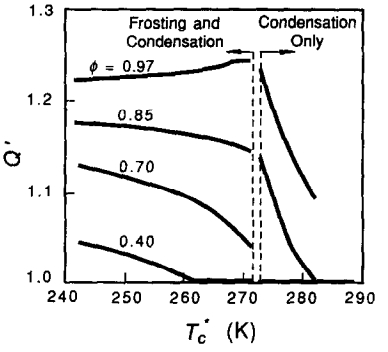

FIG. 8. The effect of cold temperature T_c^* on the quasi-steady-state heat flux ratio for different ambient relative humidities: $\varepsilon_{\beta 0} = 10^{-7}$.

length of the frozen region directly affects the temperature gradient and its increase reduces the heat flux. In the meantime, the effective thermal conductivity increases as moisture/frost contents increase, which results in an increase in Q'. Therefore, for high humidity cases, the dominant factor that influences the Q'–T_c behavior is the temperature gradient in the frozen region, which decreases with T_c; while for low humidity cases ($\phi < 0.85$), the increase in k_{eff} due to frost accumulation dominates, which explains the increase in Q' with the decrease in T_c.

By inspection of Fig. 8, it can be concluded that for $\phi < 0.40$, no significant effects of condensation or frosting on the heat loss through the insulation slab exists under quasi-steady-state conditions. The insulation behaves like a dry material even though the cold temperature drops well below 273 K. Condensation and frosting effects would lead to a maximum 30–40% increase in heat loss. This suggests that as long as the basic mode for moisture transport inside an insulation slab is vapor diffusion, the effects of liquid/frost accumulation on thermal performance is not significant. This confirms the importance of using a good vapor retarder to minimize air infiltration. It should be mentioned that since the trend in Q'–T_c^* for the process with condensation and frosting is different than the process with condensation only ($T_c^* > 273$ K), theoretically, the curve shown in Fig. 8 may not be continuous at the temperature which distinguishes between the two processes.

5. CONCLUSIONS

The following conclusions may be drawn for a typical glass-fiber insulation slab:

(1) After the process reaches a quasi-steady state, the maximum moisture accumulation occurs near the boundary between the frozen and wet regions, which is unlike the process without frosting that has the maximum accumulation always near the cold impermeable boundary.

(2) As long as liquid is in the pendular state, the initial liquid volume fraction $\varepsilon_{\beta 0}$ does not substantially affect the temperature field in the insulation slab, but would cause a significant increase in the effective thermal conductivity for $\varepsilon_{\beta 0} \geqslant 0.005$; therefore, results in an increase in Q'.

(3) The frost accumulation results in an increase in the heat flux ratio, Q', as compared to the process when only condensation takes place, if the ambient relative humidity is approximately above 0.40.

(4) For a moderate ambient humidity level ($0.40 \leqslant \phi \leqslant 0.90$) and otherwise the same boundary and initial conditions, a slab subject to a lower subfreezing temperature has a larger frozen region length and larger heat flux ratio, Q'. A slab, with one side open to a moist air close to 100% relative humidity, may have a smaller heat flux ratio as its cold boundary temperature (below 273 K) decreases.

REFERENCES

1. E. R. G. Eckert and M. Faghri, A general analysis of moisture migration caused by temperature differences in an unsaturated porous medium, *Int. J. Heat Mass Transfer* **23,** 1613–1623 (1980).
2. D. A. de Vries, The theory of heat and moisture transfer in porous media revisited, *Int. J. Heat Mass Transfer* **30,** 1343–1350 (1987).
3. A. P. Shapiro and S. Motakef, Unsteady heat and mass transfer with phase change in porous slabs: analytical solutions and experimental results, *Int. J. Heat Mass Transfer* **33,** 163–173 (1990).
4. C. Langlais, M. Hyrien and S. Karlsfeld, Moisture migration in fibrous insulating material under the influence of a thermal gradient. In *Moisture Migration in Buildings*, ASTM STP 779, pp. 191–206 (1982).
5. N. E. Wijeysundera, M. N. A. Hawlader and Y. T. Tan, Water vapor diffusion and condensation in fibrous insulations, *Int. J. Heat Mass Transfer* **32,** 1865–1878 (1989).
6. K. Vafai and S. Sarker, Condensation effects in a fibrous insulation slab, *J. Heat Transfer* **108,** 667–675 (1986).
7. K. Vafai and S. Whitaker, Simultaneous heat and mass transfer accompanied by phase change in porous insulation, *J. Heat Transfer* **108,** 132–140 (1986).
8. H. Auracher, Water vapor diffusion and frost in porous materials. In *Heat Transmission Measurements in Thermal Insulations*, ASTM STP 544, pp. 49–67 (1974).
9. J. P. Gupta and S. W. Churchill, A model for the migration of moisture during the freezing of wet sand, *A.I.Ch.E. Symp. Ser.* **69**(131), 192–198 (1972).
10. Y. C. Fey and M. A. Boles, The parametric analysis of self-freezing in an initially wet porous medium, *Int. J. Heat Fluid Flow* **9,** 147–155 (1988).
11. S. Whitaker, Simultaneous heat, mass and momentum transfer in porous media: a theory of drying. In *Advances in Heat Transfer* (Edited by J. P. Hartnett and T. F. Irvine, Jr.), Vol. 13. Academic Press, New York (1977).

TRANSFERT VARIABLE DE CHALEUR ET DE MASSE AVEC CHANGEMENT DE MASSE DANS UNE COUCHE ISOLEE: EFFETS DU GEL

Résumé—L'humidité et l'accumulation de gel dans une couche de fibre de verre sont analysées en utilisant un modèle monodimensionnel, de diffusion variable de vapeur avec changement de phase et propriétés variables. La frontière de puit froid est imperméable et fixée à une température inférieure au point triple de l'eau tandis que la paroi opposée chaude est ouverte à une convection d'air humide. Les résultats numériques sont présentés pour l'accumulation d'humidité/de gel dans des conditions variées. On montre que le mouvement de la frontière gelée est principalement gouverné par la diffusion thermique. On discute aussi les effets de ces accumulations sur la performance thermique.

INSTATIONÄRE WÄRME- UND STOFFÜBERTRAGUNG MIT PHASENWECHSEL IN EINER ISOLIERSCHICHT—REIF-EFFEKTE

Zusammenfassung—Mit Hilfe eines eindimensionalen instationären Modells für die Dampfdiffusion mit Phasenwechsel und variablen Stoffeigenschaften wird die Feuchtigkeits- und Reifansammlung in Fiberglasschichten analysiert. Die Begrenzung an der kalten Seite ist undurchlässig und wird auf einer Temperatur unterhalb des Tripelpunkts von Wasser gehalten, während die warme Grenzfläche durchlässig ist und von feuchter Luft überströmt wird. Die Ansammlung von Feuchtigkeit und Reif wird für unterschiedliche Bedingungen numerisch berechnet. Es zeigt sich, daß die Bewegung der Gefrierfront hauptsächlich durch Wärmeleiteffekte bestimmt wird. Die Einflüsse der Feuchtigkeits-/Reif-Ansammlung auf das thermische Verhalten wird ebenfalls untersucht.

НЕСТАЦИОНАРНЫЙ ТЕПЛО- И МАССОПЕРЕНОС ПРИ ФАЗОВЫХ ПЕРЕХОДАХ В ИЗОЛЯЦИОННОЙ ПЛАСТИНЕ: ЭФФЕКТЫ НАМЕРЗАНИЯ

Аннотация—С использованием одномерной нестационарной модели диффузии пара при фазовом переходе и переменных теплофизических свойствах анализируются накопление влаги и инея в пластине из стекловолокна. Граница стока холода является непроницаемой и находится при температуре ниже тройной точки воды, в то время как противоположная нагретая граница подвержена действию конвективного влажного воздуха. Приводятся численные результаты для накопления влаги/инея в различных условиях. Показано, что перемещение границы замораживания преимущественно определяется переносом тепла. Обсуждается также влияние накопления влаги/инея на теплоизоляционные характеристики.